Microfluid Nanofluid (2007) 3:151–160
DOI 10.1007/s10404-006-0115-6

RESEARCH PAPER

Electroosmotic flow in microchannels with prismatic elements

Yandong Hu · Xiangchun Xuan · Carsten Werner · Dongqing Li

Received: 5 March 2006 / Accepted: 26 July 2006 / Published online: 16 September 2006

Abstract Fundamental understanding of liquid flow through microchannels with 3D prismatic elements is important to the design and operation of lab-on-a-chip devices. In this paper, we studied experimentally and theoretically the electroosmotic flow (EOF) in slit microchannels with rectangular 3D prismatic elements fabricated on the bottom channel wall. The average electroosmotic velocity measured by the current-monitoring technique was found lower than that in a smooth microchannel. This velocity reduction becomes larger in microchannel with larger but less number of the prisms even though the space taken by the prisms are identical. The velocity distribution and streamlines on two typical horizontal planes in the microchannel are measured and visualized by a particle-based technique. These experimental observations are in good agreement with the numerical simulation. The comparison of streamlines near the prisms in the pressure-driven flow with that in the EOF showed that the EOF was more sensitive to the local geometry.

Y. Hu · X. Xuan · C. Werner
Department of Mechanical and Industrial Engineering, University of Toronto, 5 King's College Road, Toronto, ON, Canada M5S 3G8

Y. Hu · C. Werner
Department of Biocompatible Materials, Institute of Polymer Research, Hohe Straβe 6, 01069 Dresden, Germany

D. Li (✉)
Department of Mechanical Engineering, Vanderbilt University, Nashville, TN 37235-1592, USA
e-mail: dongqing.li@vanderbilt.edu

1 Introduction

In many microfluidic devices, interfacial electrokinetic phenomena (Delgado 2001; Probstein 1994; Masliyah 1994; Li 2004) play important roles in liquid transport in microchannels. Particularly relevant to liquid flows in microchannels is the electrical double layer (EDL), a thin layer of liquid with excess counter-ions attracted to the surface charge of the channel walls (Delgado 2001; Li 2004). Electroosmotic flow (EOF) results from the motion of the excess counter-ions in the EDL under an axially applied electric field. There are many studies of EOF in smooth microchannels with either homogeneous surface property or with heterogeneous surface charge patches (Ren and Li 2002; Ermakov et al. 1998; Biddiss et al. 2004). However, little work has been reported on the EOF in microchannels with 3D structures. These 3D structures on microchannel walls can be produced through microfabrication to create desirable flow and surface features. For example, prismatic elements are used actively in creating streams mixing in microchannels (Biddiss et al. 2004). They can also be used to increase the bio-chemical reaction surface area in a microchannel bio-reactor for enhancing the reaction efficiency and bio-sensor sensitivity. For both cases, however, these 3D elements will inevitably influence the liquid flow and sample transport in microchannels.

Several previous studies discussed the influence of surface roughness on the friction loss in pressure-driven laminar flow in microchannels (Hu et al. 2003a, b; Papautsky et al. 1999; Mala and Li 1999). It was shown that the flow resistance is significantly higher than that predicted by the Poiesuille flow theory. Different models were proposed to simulate the flow resistance

in pressure-driven flows as a function of relative height of the surface roughness (Hu et al. 2003a, b; Papautsky et al. 1999; Mala and Li 1999). Recently, the effect of 3D prismatic elements on EOF in microchannels has been numerically investigated (Hu et al. 2003a, b). It was found that, during an EOF, there are no flow recirculation and hence no trapped sample molecules in between the 3D elements in a microchannel with homogeneous surface property. It was also found that pressure fluctuations are induced by these 3D prismatic elements in the main flow direction, and hence the flow rate is significantly reduced.

In this paper, we present an experimental study of EOF in slit microchannels with 3D prismatic elements. These elements were fabricated by a soft lithography method. The average flow velocity and the flow field distribution were investigated with the current-monitoring technique and a particle-based flow visualization technique, respectively. Moreover, the experimental data were compared with numerical simulation results.

2 Theory

We consider a slit microchannel formed by two parallel surfaces with square prismatic elements on the bottom one. Figure 1 illustrates the two types of arrangements of prismatic elements on the bottom channel wall to be investigated: (a) symmetrical and (b) asymmetrical. The parameters describing such a microchannel of either type include: (1) the prismatic elements' size, a; (2) the element's height, h; (3) the separation distance, b, between adjacent elements; and (4) the microchannel height, H. We neglect the entrance effect and the edge effect, and assume fully developed periodical flows through the microchannel. Since the flow behavior repeats in each period, the space of one flow period is chosen as the computational domain, i.e., the region between two symmetrical planes with one element separation distance, as shown in Fig. 1.

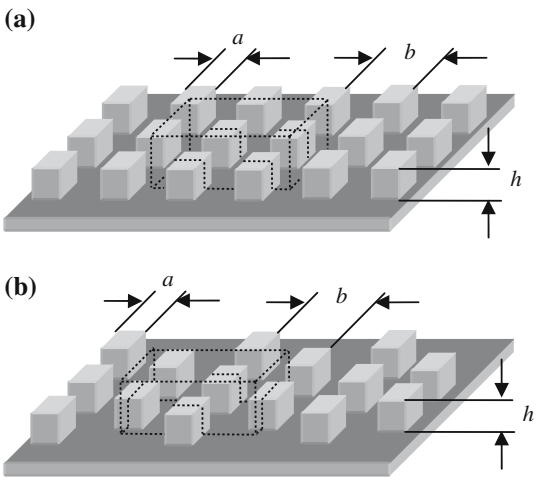

Fig. 1 Illustration of the bottom microchannel wall with two types of arrangements of prismatic elements: **a** symmetrical and **b** asymmetrical. The parameters to prescribe the rough channel (not to scale) are: a is the size of the prismatic element, h is the height, b is the separation distance between adjacent elements, and H is the height of the microchannel

The governing equations for the applied electrical field and the flow field are given by (Hu et al. 2003a, b)

$$\tilde{\nabla}^2\phi = 0, \tag{1}$$

$$\tilde{\nabla}\cdot\tilde{V}_{\mathrm{eo}} = 0, \tag{2}$$

$$\rho\left(\tilde{V}_{\mathrm{eo}}\cdot\tilde{\nabla}\right)\tilde{V}_{\mathrm{eo}} = -\tilde{\nabla}p + \mu\tilde{\nabla}^2\tilde{V}_{\mathrm{eo}}, \tag{3}$$

where ϕ is the applied electrical potential, $\tilde{V}_{\mathrm{eo}}$ is the electroosmotic velocity, p is the pressure, ρ is the liquid density, and μ is the liquid viscosity. The effect of electric driven force on the flow in the EDL is considered by the slip boundary condition at the solid–liquid interface.

$$\tilde{V}_{\mathrm{eo,slip}} = \frac{\varepsilon\zeta}{\mu}\tilde{E}, \tag{4}$$

where ϵ is the dielectric constant of the liquid, ζ is the zeta potential of the solid–liquid interface, and $\tilde{E}$ is the applied electrical field. To solve the flow field, the symmetry boundary condition is applied to the side face of the computational domain. Fully developed periodic boundary condition is applied to the inlet and outlet faces of the computational domain. To solve the electrical potential field, the EOF field and the concentration field during the species transport process numerically, we developed a 3D-computation code based on the finite volume approach (Patankar 1980) and SIMPLEC algorithm (Patankar 1980). The first order upwind numerical scheme was applied to solve the 3D electrical field and the Navier–Stokes equation. A 3D structured grid system was applied to our computational domain. Grid-independence was examined for two different grids whose total cell numbers were 22,190 and 44,380, respectively. The calculated flow rates difference was less than 1% by using the two grids. Therefore, the grid independence was reached, and the grid with 22,190 cells was applied in the study. The details of solving Eqs. 1, 2 and 3 for the electrical field and the flow field can be found elsewhere (Hu et al. 2003a, b). Through solving Eqs. 2 and 3, the flow field $\tilde{V}_{\mathrm{eo}}$can be obtained. However, when charged micro-particles move with the flow, the charged

particles also experience the electrophoretic force. The equation of particle's electrophoretic motion relative to the fluid becomes (Delgado 2001) $\tilde{V}_{ep} = -\varepsilon\xi_{particle}\,\tilde{E}/\mu$. Therefore, the particle's absolute velocity is

$$\tilde{V}_{particle} = \tilde{V}_{eo} + \tilde{V}_{ep} \tag{5}$$

3 Experiments

3.1 Fabrication of microchannels with rectangular prismatic elements

The microchannels with rectangular prismatic elements were fabricated using a soft lithography rapid prototyping technique (Duffy et al. 1998; Becker and Gärtner 1999). The procedure is schematically shown in Fig. 2. In the first step, a thin layer of SU-8 photoresist (MicroChem Cop., Newton, MA, USA) was spin coated on a glass slide to a desired thickness. The resultant photoresist film was then exposed to UV light through a photo mask. Two types of masks were used as illustrated in Fig. 2a: one is for making the smooth side of the channel (left subplot), and the other is for making the prismatic elements (right subplot). After dissolving the unwanted photoresist in the developer solution (Sigma-Aldrich, St. Louis, MO, USA), two masters were obtained as seen in Fig. 2b. Following that, liquid PDMS, which was prepared by thoroughly mixing Sylgard 184 and the curing agent (Dow Corning, Midland, MI, USA) at a 10:1 ratio in weight, was poured over the masters and cured in vacuum for 3–4 h. The two negative PDMS casts of the microchannel patterns as shown in Fig. 2c were then removed from the masters and bonded to each other immediately after the plasma treating (PDC-32G, Harrick Scientific, Ossining, NY, USA). The final

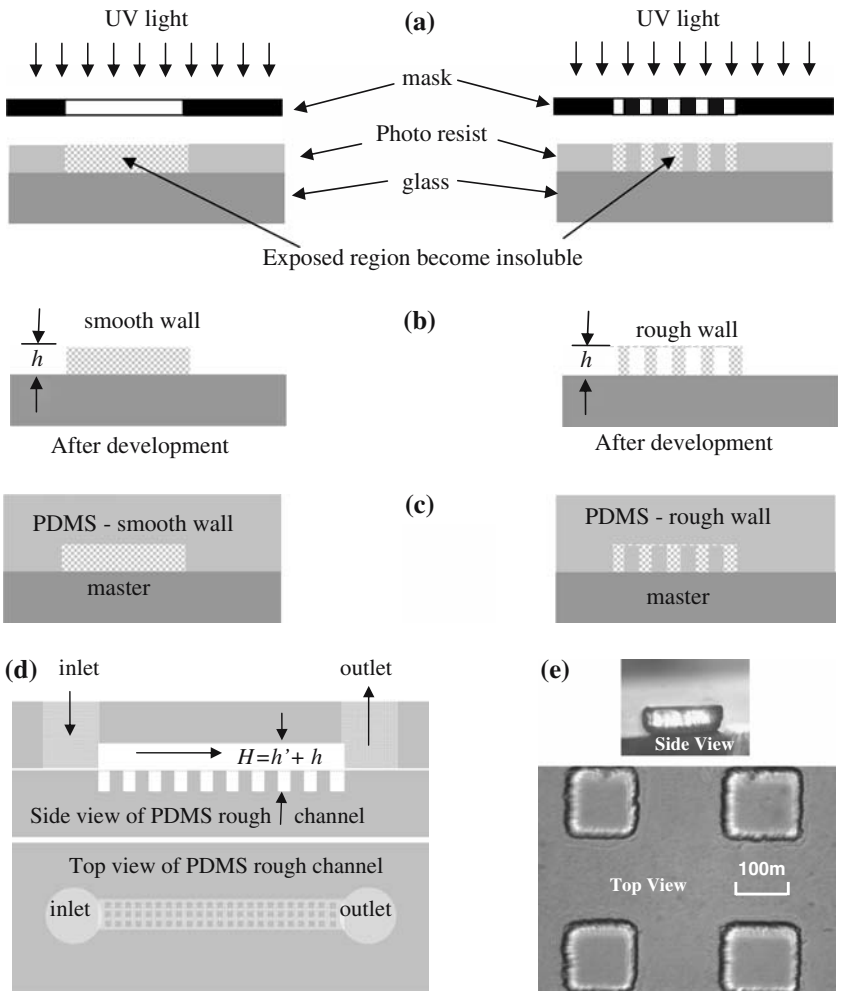

Fig. 2 Soft-lithography based rough microchannel fabrication procedure: **a** photo mask design and UV light exposure, **b** formation of the masters, **c** PDMS casting, **d** PDMS rough channel aligning and sealing, **e** Sample rough microchannel

structure of the microchannel with prismatic elements on the bottom channel wall is displayed in Fig. 2d. A close-up top view of these prismatic elements is given in Fig. 2e where the upper photo was viewed from the side.

3.2 Measurement of average electroosmotic velocity

An indirect method based on monitoring the electrical current change was used to measure the average electroosmotic velocity in the tested microchannels (Huang et al. 1988; Ren et al. 2002). Generally most EOFs, owing to the inherently low Reynolds number, reach a steady state very quickly (in a few milli seconds) and the entrance length tends to be extremely short. Therefore the flow could be assumed as steady, fully developed. The channel was initially filled with 0.5 mM sodium carbonate buffer and then brought into contact with 0.45 mM sodium carbonate buffer at the same time, an electrical field was applied in such a way that 0.45 mM buffer was pumped into the channel, replacing 0.5 mM buffer. The slightly lower concentration electrolyte solution from inlet reservoir migrates into the microchannel, displacing an equal volume of a higher concentration electrolyte solution. The small concentration difference ensures essentially the same EOF velocity for the two solutions, but a sensible fluid conductivity difference between these two liquids. As a consequence, the total electrical resistance of the liquid in the microchannel changes and hence the current decreases. Once the higher concentration solution in the channel is completely replaced by the lower concentration solution from the inlet reservoir, the current will reach a constant minimum value. The time for the current to reach this constant value is the time required for the lower concentration solution to complete the filling of the microchannel at a steady, fully developed velocity. The EOF velocity can be estimated by dividing the channel length by this solution replacing time, given by

$$\bar{U}_{\mathrm{eo}} = \frac{L}{\Delta t}, \tag{6}$$

where L is the length of the channel, and Δt is the time required for the completion of the solution replacement (determined from the measured current data). This experiment was repeated in both smooth and the designed channels. For our specific microchannels, the average cross-sectional velocity varies periodically, corresponding to the variations of the cross-sectional area. As a result, the average displacing velocity in the microchannel, $\overline{\bar{U}}_{\mathrm{eo}}$, can be represented numerically by the mean value of the average cross-sectional velocity in one flow period, as given below:

$$\overline{U}_{\mathrm{eo}} = \frac{1}{l}\sum_{l}\left(\frac{\sum_{A_c} u \cdot \Delta y \Delta z}{\sum_{A_c} \Delta y \Delta z}\right)\Delta x, \tag{7}$$

where A_c is the local cross-sectional area; l is the length of one flow period.

3.3 Visualization of EOF field

The recently developed μ-PIV technique (Meinhart et al. 1999, 2000) was employed to measure the EOF field in microchannels with prismatic elements. In the experiments, polystyrene fluorescent microspheres (Bangs Laboratories, Inc., IN, USA) of 1 μm in diameter were used as the tracing particles. The microsphere suspension as received was diluted 25 times by volume with pure water before use. An Argon laser (λ = 488 nm) was used to excite continuously the fluorescence on the microspheres. After being collected by a 32×, NA (numerical aperture) = 0.60 microscope objective, the emitted fluorescent signal was recorded by a progressively scanning CCD camera running in video mode at 15 fps (frame per second). The estimated depth of field for our optic system is ~20 μm (Meinhart et al. 1999; Inoue and Spring 1997). By adjusting the vertical position of the focus plane of the microscope objective, particle images on two horizontal planes were taken: one is at the half height of the prismatic elements, and the other is at the half height of the free space above the prismatic elements. The acquired images (viewed from the top) had a resolution of 640 × 480 pixels and an 8-bit dynamic range. The particles that are out of focus show relatively low light intensity compared with those in focus, they were removed from the images using a Matlab program. For the analysis of the PIV images and the extraction of the velocity vectors, the method of cross-correlation between two sequential frames was implemented using commercial software (AEA VISIFLOW©). The vectors are placed on a uniform Cartesian grid with dimensions of 30 × 40. The image acquisition frame rate was set at 15 fps. Fluorescent particle aggregation would significantly change the electrophoretic mobility or the surface property. Cummings and Lapizco-Encinas et al. (Cummings and Singh 2003; Lapizco-Encinas et al. 2004, 2005) found that the particles can be concentrated or even trapped in microchannels containing arrays of posts under high

electrical field strength, for example 200 KV/m in some references (Cummings and Singh 2003; Lapizco-Encinas et al. 2004, 2005). However, this phenomenon is not eminent when electrical field strength is small or the particle size is small (Jones 1995). To avoid this phenomenon in our experiments, low electric field strength (i.e., 10 KV/m) and small particle (i.e., 1 μm) were employed. Additionally, before conducting our experiments, the microchannel was flushed with particle solutions so that the aggregation and adsorption were mostly avoided.

4 Results and discussion

4.1 Average electroosmotic velocity

Figure 3 compares the experimentally measured and numerically predicted average EOF velocities $\bar{U}_{eo}$ versus the applied electric field strength in channels with symmetric prismatic elements. Those velocities in a smooth channel are also shown in Fig. 3 as a reference. Note that in the numerical simulation, the zeta potential at the solid–liquid interface in both smooth and rough channels was determined from the measured $\bar{U}_{eo}$ in the smooth microchannel with the well-known Helmhotlz–Smoluchowski equation (Delgado 2001). One can see a good agreement between the experimental and numerical results. As expected, $\bar{U}_{eo}$ is a linear function of the applied electrical field strength for both the smooth channel and the channels with prismatic elements. However, $\bar{U}_{eo}$ in the channels with the prismatic elements is lower than that in the smooth channel. Moreover, $\bar{U}_{eo}$decreases with the increase of the elements' size. Our previous numerical analysis has shown that the reduction of the average electroosmotic velocity is caused by the prisms-induced local pressure fluctuations that are absent in smooth microchannels (Hu et al. 2003a, b). In microchannels with prismatic elements on the wall, pressure fluctuations are induced when EOF encounters these prisms, i.e., higher pressure regions appear at the front of the element and lower pressure zone appear at the tail region. Hence, the high pressure zone at the elements' front region tends to resist the flow from moving forward; the low pressure zone at the tail region tends to expand the fluid to the element's tail region. The average flow velocity in the main stream direction is then reduced by the resistance and the expansion in the microchannels. The fraction of the average velocity reduction is ultimately dependent on resistance induced by the prismatic elements (Hu et al. 2003a, b).

The prisms' separation distance decides the number of the prism in the microchannel with the same width and length. The ratio of the prismatic elements' size to the separation distance (a/b) determines the fraction of the space taken by the prismatic elements in the microchannel. The larger a/b is, the greater the space

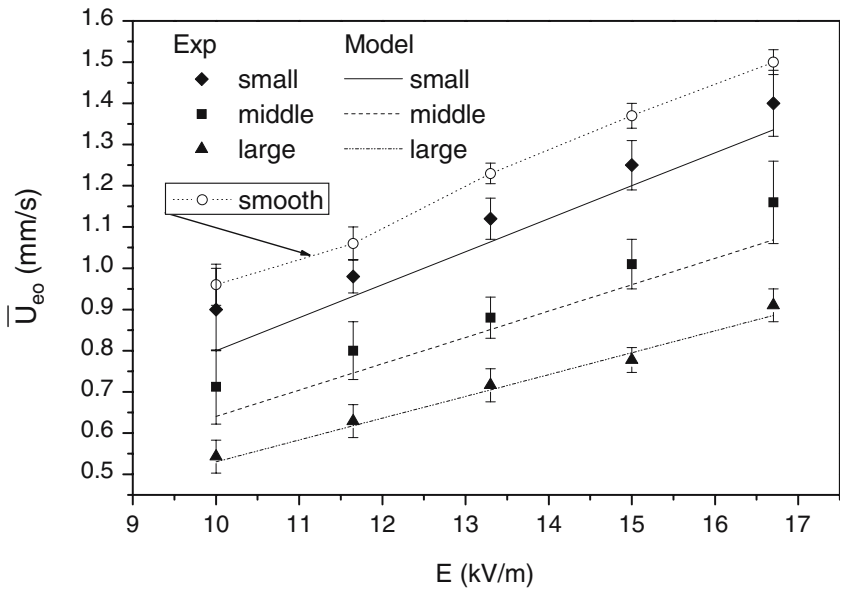

Fig. 3 The average electroosmotic flow (*EOF*) velocity measured by the current-monitoring method in a smooth channel ($H \times W \times L = 20\ \mu m \times 2\ mm \times 30\ mm$) and three microchannels ($H \times W \times L = 40\ \mu m \times 2\ mm \times 30\ mm$) with prismatic elements with parameters: (1) small size element: $h = 20\ \mu m$, $a = 50\ \mu m$ and $b = 250\ \mu m$; (2) middle size element: $h = 20\ \mu m$, $a = 100\ \mu m$ and $b = 500\ \mu m$; (3) large size element: $h = 20\ \mu m$, $a = 250\ \mu m$ and $b = 500\ \mu m$

taken by the prismatic elements in a given microchannel (i.e., a given set of channel length, width and a given prisms height). When one increases the prism elements' size while keeping the separation distance, the space taken by the prismatic elements in the microchannel increases. Intuitively, larger blocking space would create larger pressure fluctuations and hence a larger average velocity reduction is expected. Therefore, in Fig. 3, the microchannel with large prisms exhibits smaller average velocity than that with the middle sized prism. However, for a given fraction of space blocked by the prismatic elements, such as the cases with small and the middle sized prism in Fig. 3, difference in average velocity still exists. For these two cases, the smaller prisms have a larger density (smaller separation distance), while the middle sized prisms (twice the small prism's size) have a smaller density (twice the small prism's separation distance). Both the numerical and the experimental data show that the one with larger elements' size and a lower density exhibit a larger average velocity reduction. This is due to the middle-sized prisms creating larger pressure fluctuations per unit cross sectional area and larger flow pattern deformations than the two separate small prisms. Such larger flow resistance results in larger average velocity reduction.

4.2 Electroosmotic velocity distribution and streamlines

Figure 4 shows the particle's velocity distributions in a microchannel with symmetric prismatic elements obtained from the μ-PIV experiment and the numerical simulation, respectively. In order to compare the particle velocity field measured by PIV technique with the model predictions, we considered the local electrophoretic velocity of the micro-particles [defined by

$$\tilde{V}_{\mathrm{ep}} = -\varepsilon\xi_{\mathrm{particle}}\tilde{E}/\mu = \mu_{\mathrm{ep}}\tilde{E}$$

(Delgado 2001)] in the simulation according to Eq. 5. The electrophoretic mobility of the particles, μ_{ep}, is approximately -2×10^{-8} m^2/Vs (Elimelech and O'Melia 1990). It is relatively small compared with the liquid electroosmotic mobility which is approximately 7.8×10^{-8} m^2/Vs. The focusing plane was at a half height of the prismatic elements. Note that the size of the numerical flow field shown in Fig. 4 has been adjusted to fit the experiment's view field which is larger than one flow period. As predicted by the numerical simulation, there is no vortex or flow recirculation at the elements' tail regions. The velocity in the pathway formed between two neighboring elements along the channel width direction is much larger than the velocity in the gaps formed between two neighboring elements along the channel length direction. This flow feature is attributed to the larger electrical field strength in the narrow passage due to the prismatic elements blocking the part of the microchannel and the local pressure drop along the pathway as well. Moreover, the latter creates the mild parabolic velocity profile in the pathway.

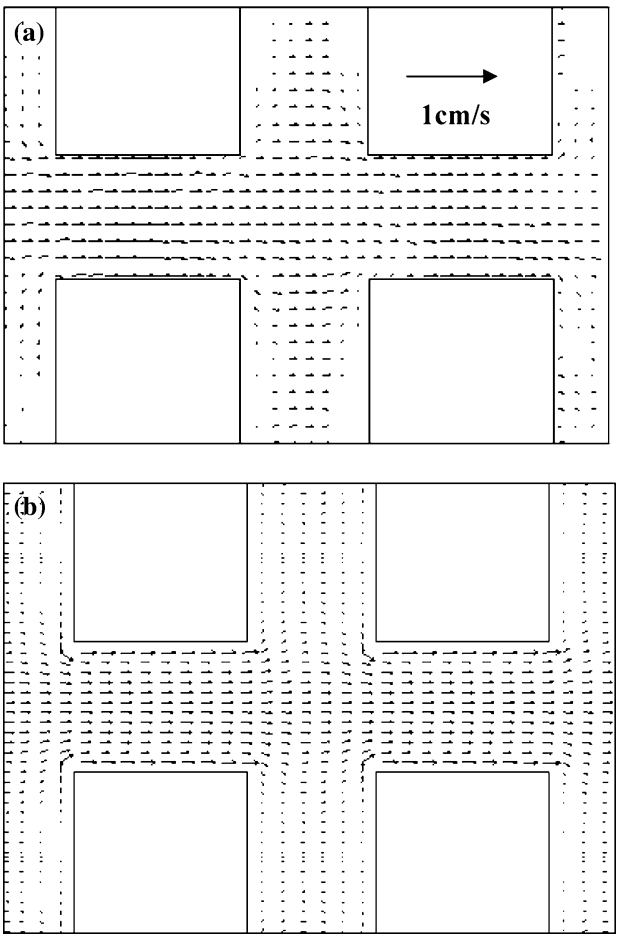

Fig. 4 Comparison of the particle velocity distribution in microchannel with symmetrical arranged prisms obtained from PIV experiment and the prediction from our numerical model: **a** experimental data and **b** the corresponding numerical velocity distribution in the plane half height of the prismatic elements. The parameters of the rough microchannel are a = 168 μm and b = 300 μm, h = 70 μm and H = 140 μm. The vector length scale is identical in all the figures

Accordingly, the EOF field in the microchannel with asymmetric prismatic elements is displayed in Fig. 5. Due to the prism's asymmetrical arrangement, the flow has more space to develop in the tail region than that in the symmetrical case. In symmetrical arrangement, when the prismatic elements separation distance is relatively small, the next element's front surface is still in the previous element's flow tail region. For example,

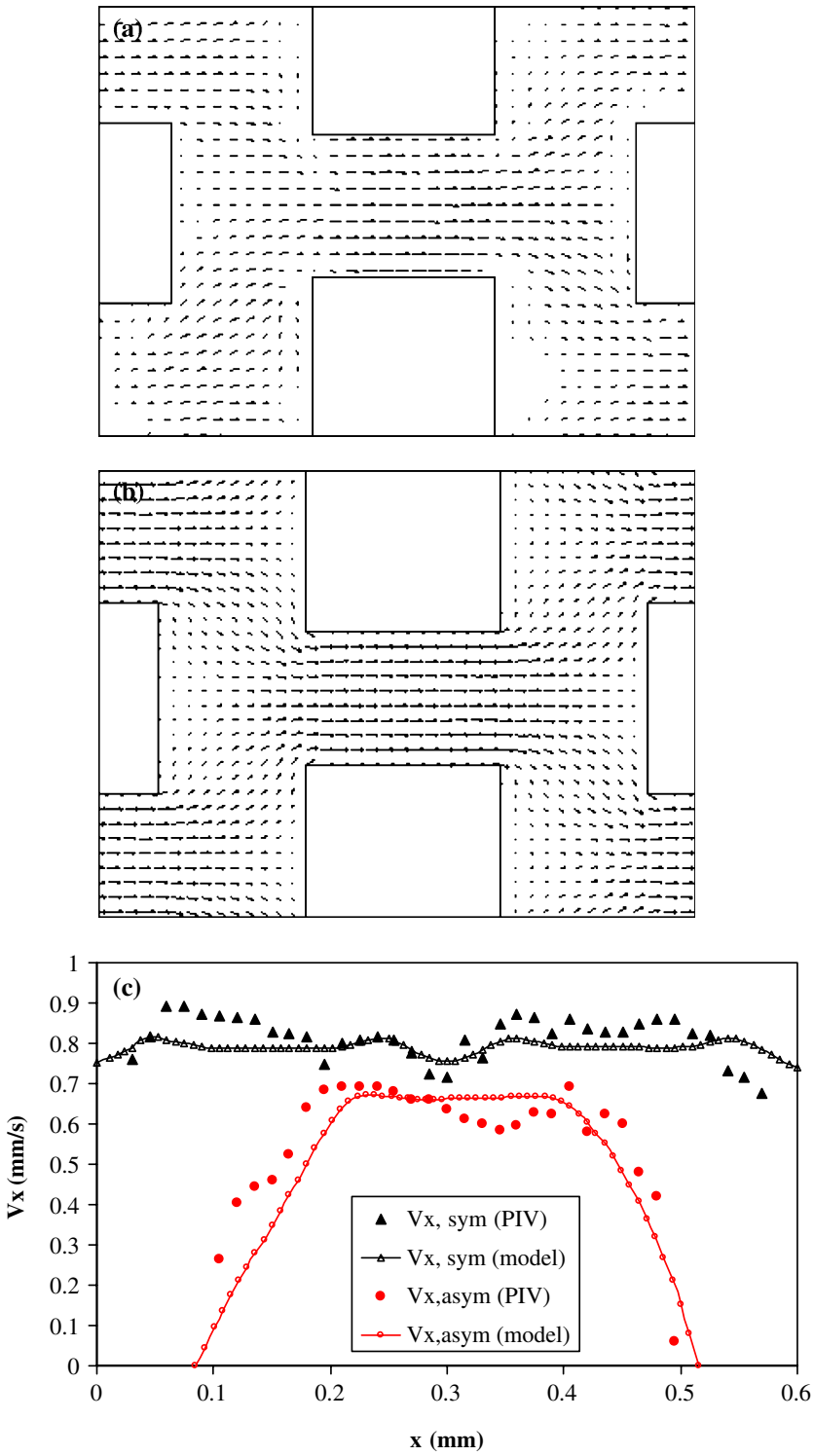

Fig. 5 Comparison of the particle velocity distribution in microchannel with asymmetrical arranged prisms obtained from PIV experiment and the prediction from our numerical model: **a** experimental data and **b** the corresponding numerical velocity distribution in the plane half height of the prismatic elements. The parameters of the rough microchannel are a = 168 μm and b = 300 μm, h = 70 μm and H = 140 μm. The vector length scale is identical to that in Fig. 4. **c** Quantitative comparison of the velocity component of the main flow direction on the symmetrical line along the main flow direction of Figs. 4a, b, 5a and b

in the situation shown in Fig. 4, the streams are not completely reunited in the tail region before they are separated again by the next prismatic element.

As a quantitative measurement of the flow field, we compared the PIV velocity component parallel to x-axis on the symmetrical line in the middle of the flow sub-channel in Figs. 4a and 5a with the results of our numerical model, shown in Figs. 4b and 5b. The comparisons are shown in Fig. 5c. The average and maximum deviations are 0.04 and 0.1 mm/s for channel with symmetrically arranged prisms, and 0.07 and 0.1 mm/s for channel with asymmetrically arranged prisms.

Figure 5c shows that the model predictions are in relatively good agreement with the PIV experiments.

We have also measured the EOF field in a plane half way in the free space above the symmetrically arranged prismatic elements as shown in Fig. 6. The velocity vectors in such a plane are essentially parallel to each other, indicating little effect of the prismatic elements. Because EOF is generated from the thin EDL region near the channel wall surface and the surface of the prismatic elements, the magnitude of the flow velocity is smaller in the plane far away from these solid surfaces. Similar EOF field was also found in the microchannel with asymmetrically arranged prismatic elements, which is not shown here.

To examine the difference between the pressure-driven flow and the EOF in a microchannel with prismatic elements, we conducted an experiment first using a pressure difference to drive the flow, and then switching the driving force to be an applied electrical field. In the pressure driven flow, by titrating 0.4 and 0.1 ml microsphere solution into the inlet and outlet reservoirs (1 cm in diameter), respectively, 3 mm H_2O pressure was applied across the microchannel length. After the fluid experienced 5 s pressure driven flow (in the experiments, it takes around 0.5 s to reach a steady state under the applied pressure drop and the applied electric field), the total volume transport through the microchannel was in the order of 10^{-3} ml, which is a negligible change in the fluid level in the inlet and outlet reservoirs. Then, 0.3 ml microsphere solution was added into the outlet reservoir to balance the pressure drop. At the same time, an electric potential difference was applied through the two electrodes in the two reservoirs, the fluid undergoes an EOF through the microchannel. Figure 7 shows the images of the steady state streamlines, i.e., the streaks of the 1 μm fluorescein-coated particles in a pressure-driven flow and in an EOF, respectively. It is known that the pressure-driven flow can create some circulating flow or stagnation zones in the gap (Hu et al. 2003a, b), and hence particles may be trapped in the gap. One can see that, in the pressure driven flow as shown in Fig. 7a and c, the gap region is filled with bright dots, i.e., the tracer particles with low speed. This implies that in the pressure driven flow, possible stagnation or small circulation occurs in the gap region. Then, after the pressure difference was removed (as described above), an electric field was applied, and a steady state EOF was established immediately (in less than a second). Figure 7b and d show the images of the steady state EOF streamlines. In the EOF, one can see that the tracer particles are moving around the prisms at a speed comparable to the central flow. Due to the induced pressure in the gap in the EOF through these prisms, the tracer particles are pushed apart in some regions, resulting some black areas in the gap region (i.e., no fluorescent particles in these locations) as seen in Fig. 7b and d. These images clearly show that there are no particles trapped in the gaps. In other words, when the EOF started, the particles trapped in the gaps were all removed from the gaps and flow to the downstream. It also can see from the pressure driven flow and the EOF through microchannel with asymmetrical element's arrangement (Fig. 7c, d) that the pressure driven flow is more sensitive than that of the EOF to the flow passage history and the passage in the downstream. In pressure driven flow through the prismatic elements, more fluid mass transfer through the passage with less overall resistance along all the

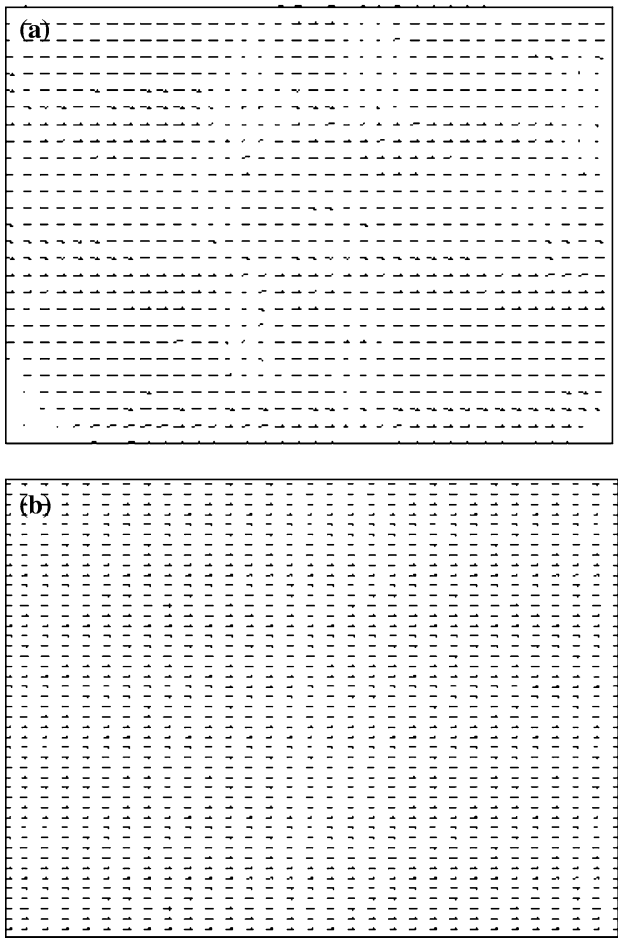

Fig. 6 Comparison of the particle velocity distribution in microchannel with symmetrical arranged prisms obtained from PIV experiment and the prediction from our numerical model: **a** Experimental data and **b** the corresponding numerical velocity distribution in the plane half height of the free region over the elements. The parameters of the rough microchannel are $a = 168$ μm and $b = 300$ μm, $h = 70$ μm and $H = 140$ μm. The vector length scale is identical to that in Fig. 4

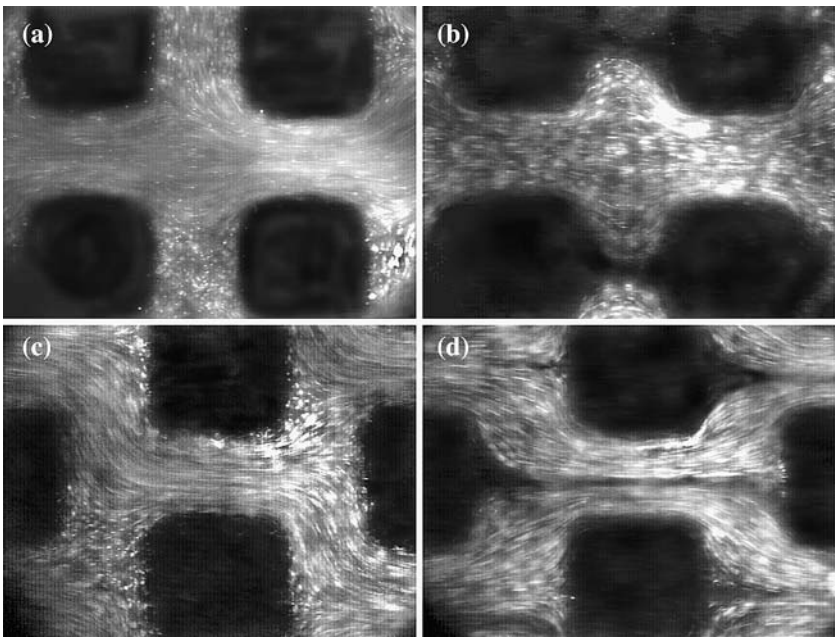

Fig. 7 Comparison of pressure-driven flow patterns (**a**) and (**c**) with electrokinetically driven flow patterns (**b**) and (**d**) through microchannels with symmetrically (**a**, **b**) and asymmetrically (**c**, **d**) arranged prismatic elements. The parameters of the rough microchannel are a = 116 μm and b = 300 μm, h = 70 μm and H = 140 μm

subchannels. The microchannel with asymmetrical element's arrangement exhibits less overall resistance along the upper-right and lower-left subchannels in the Fig. 7, and hence a major stream passes through the microchannel in tilted direction. However, at the same observed spot in the same microchannel, EOF demonstrates a quite symmetry in Fig. 7d.

The numerically simulated top view of the streamlines of the EOF in the microchannels with symmetrically and asymmetrically arranged elements were shown in Fig. 8a and b, respectively. In comparison with the experimental streamline images shown in Fig. 7b and d, the simulations are in good agreement with the experiments, and clearly show that there are no flow circulations in the gap regions.

5 Conclusions

In this paper, experimentally, we used the current-monitoring technique and the particle tracking technique to study the flow field and the mass transport in microchannels with prismatic elements. The current-monitoring technique measures the average velocity in the microchannels with prismatic elements. The results show that the average velocity is proportional to the applied electrical voltage over the microchannels with prismatic elements, and is smaller than that in a smooth microchannel. Different average velocity reductions are shown with different element's configurations. The pressure fluctuation induced by the prismatic elements contributes to the velocity reduction. Using the particle tracking technique, we obtained the velocity distributions on two specific horizontal planes in the microchannels and the direct images of streamlines. The results are in good agreement with the numerical model. Comparing the streamline images of the pressure-driven flow with that of the EOF, one can clearly see that the particles are trapped in the gap regions in pressure driven flow; however this behavior does not exist in EOF.

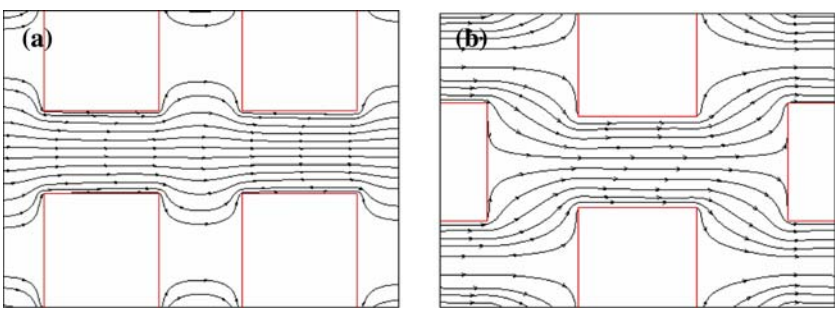

Fig. 8 Model predicted streamlines of EOF through rough microchannels for the two experimental rough microchannels in Fig. 7: **a** rough microchannel with symmetrical arrangement and **b** with asymmetrical arrangement

Acknowledgments The authors are thankful for the financial support of the Institute for Polymer Research Dresden to Y. Hu, and the support of a Research Grant of the Natural Sciences and Engineering Research Council of Canada, and a Research Grant of the Canadian Institute of Photonic Innovation to D. Li. The authors also thank Mr. Wenhua Zhong for treating the PIV data.

References

Becker H, Gärtner C (1999) Polymer microfabrication methods for microfluidic analytical applications. Electrophoresis 21:12–26

Biddiss E, Erickson D, Li D (2004) Heterogeneous surface charge enhanced micro-mixing for electrokinetic flows. Anal Chem 76:3208–3213

Cummings EB, Singh AK (2003) Dielectrophoresis in microchips containing arrays of insulating posts: Theoretical and experimental results. Anal Chem 75(18):4724–4731

Delgado AV (2001) Interfacial electrokinetics and electrophoresis. Marcel Dekker, New York

Duffy D, McDonald J, Schueller O, Whitesides G (1998) Rapid prototyping of microfluidic systems in poly(dimethylsiloxane). Anal Chem 70:4974–4984

Elimelech M, O'Melia CR (1990) Effect of electrolyte type on the electrophoretic mobility of polystyrene latex colloids. Colloids Surf 44:165–178

Ermakov SV, Jacobson SC, Ramsey JM (1998) Computer simulations of electrokinetic transport in microfabricated channel structures. Anal Chem 70:4494

Hu Y, Werner C, Li D (2003a) Influence of three-dimensional roughness on pressure-driven flow through microchannels. J Fluids Eng 125:871–879

Hu Y, Werner C, Li D (2003b) Electrokinetic transport through rough microchannels. Anal Chem 75:5747–5758

Huang X, Gordon MJ, Zare RN (1988) Current-monitoring method for measuring the electroosmotic flow rate in capillary zone electrophoresis. Anal Chem 60:1837

Inoue HS, Spring KR (1997) Video microscopy, 2nd edn. Plenum Press, Oxford

Jones TB (1995) Electromechanics of particles. Cambridge University Press, Cambridge

Lapizco-Encinas BH, Simmons BA, Cummings EB, Fintschenko Y (2004) Insulator-based dielectrophoresis for the selective concentration and separation of live bacteria in water. Electrophoresis 25(10–11):1695–1704

Lapizco-Encinas BH, Davalos RV, Simmons BA, Cummings EB, Fintschenko Y (2005) An insulator-based (electrodeless) dielectrophoretic concentrator for microbes in water. J Microbiol Methods 62(3):317–326

Li D (2004) Electrokinetics in microfluidics. Elsevier, Amsterdam

Mala GM, Li D (1999) Flow characteristics of water in microtubes. Int J Heat Fluid Flow 20:142–148

Masliyah JH (1994) Electrokinetic transport phenomena. AOSTRA, Edmonton

Meinhart CD, Wereley ST, Santiago JG (1999) PIV measurements of a microchannel flow. Exp Fluids 27(5):414–419

Meinhart CD, Wereley ST, Santiago JG (2000) A PIV algorithm for estimating time-averaged velocity fields. J Fluids Eng 122:285–289

Papautsky I, Brazile J, Ameel T, Frazier AB (1999) Laminar fluid behavior in microchannels using micropolar fluid theory. Sens Actuators A 73:101–108

Patankar SV (1980) Numerical heat transfer and fluid flow. Hemisphere, Washington

Probstein RF (1994) Physicochemical hydrodynamics. 2nd edn. Wiley, New York

Ren L, Li D (2002) Theoretical studies of microfluidic dispensing processes. J Colloid Interface Sci 254:384

Ren L, Escobedo C, Li D (2002) A new method of evaluating the average electro-osmotic flow, J Colloid Interface Sci 250:238–242